EXPERIMENTAL STUDY ON DEFECTS DETECTION IN GFRP LAMINATES USING LOCK-IN INFRARED THERMOGRAPHY TECHNOLOGY

by

Qing-Ju TANG*, Ze-Shen QU, Gui-Peng XU, and Xin-Jie TAN

School of Mechanical Engineering,
Heilongjiang University of Science and Technology, Harbin, China

Original scientific paper
https://doi.org/10.2298/TSCI230611041T

To detect the debonding defect of glass fiber reinforced polymer (GFRP) laminate, the lock-in infrared thermography non-destructive testing system is built and the systematic testing research are conducted, and the effect of different geometrical parameters of debonding defects on the testing results are analyzed. Algorithms such as inter frame differential-multi frame cumulative average method, polynomial fitting-correlation coefficient method, and time-difference contrast method are used to process the image sequence, and signal-to-noise ratio and information entropy are defined as the parameters for evaluating the performance of algorithms.

Key words: *glass fiber reinforced polymer laminate, infrared thermography, image sequence, signal-to-noise ratio, information entropy*

Introduction

The GFRP as one of the common combined materials, has the advantages of light weight, corrosion preventive, good chemical stability*, etc.* So, it is used in many industrial fields, including but not limited to construction, transportation, aerospace, energy and other fields [1].However, in the production and use of GFRP laminates, due to the existence of various factors, which ultimately lead to fiber-reinforced composite products are prone to debonding defects, and a major safety hazard is caused [2]. Therefore, in order to find the internal defects of GFRP laminates in time, ensure the integrity of its structure, it is necessary to conduct non-destructive testing of GFRP laminates.

Based on the principle of infrared radiation, infrared thermal imaging non-destructive testing [3, 4] is a non-destructive testing method developed in recent years. It is characterized by fast testing speed, non-contact, non-pollution, and sensitivity to near-surface defects and features of components [5, 6].

Infrared thermal imaging test

Principle of detection

Figure 1 shows the diagrammatic sketch of the testing system, which mainly includes the thermal excitation system, the image acquisition system, the image analysis and processing system. The principle is that the heat transformation causes a temperature change on the surface

* Corresponding author, e-mail: tangqingju@126.com

of the specimen, and the infrared camera collects the temperature signal and transmits it to a computer.

When the lock-in thermal excitation is applied to the specimen, the heat flow on the specimen surface is shown:

$$q(t) = \frac{q_0}{2}\left[1 + \sin(2\pi ft)\right],\ t \in [0, T] \tag{1}$$

where $q(t)$ is the heat flow from halogen lamps, q_0 – the maximum heat flow output from halogen lamps, f – the phase-locked frequency, and T – the scan period of the modulation signal.

Specimen preparation

The GFRP laminate with dimensions of 140 mm × 140 mm × 5 mm was prepared and its debonding defects were simulated by drilling blind holes. Figure 2 is a practicality picture of GFRP laminate.

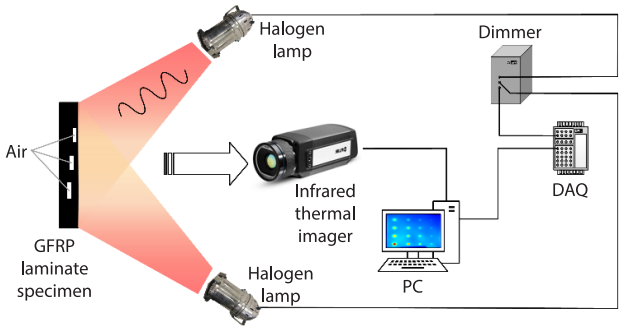

Figure 1. Testing system

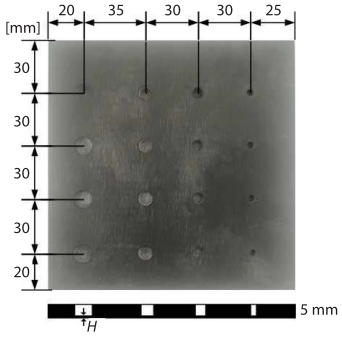

Figure 2. Practicality picture of GFRP laminate

Testing parameters

The power of the halogen lamp was set to 2000 W, the lock-in frequency was 0.05 Hz. The sampling rate of the infrared thermal imager was 20 Hz and the acquisition time is 40 seconds to acquire the surface temperature of GFRP laminate.

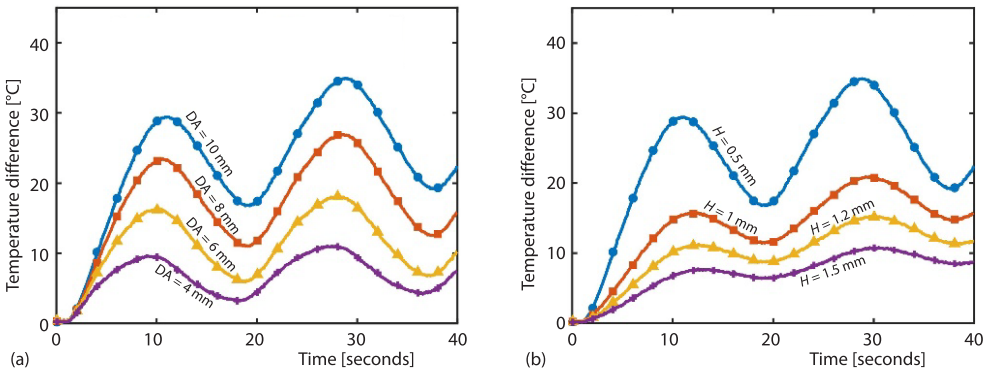

Figure 3. Temperature difference of surface; (a) different defect diameters and (b) different defect depths

Testing results and analysis

Effect of geometrical parameters of defects on surface temperature difference

Figure 3 shows the effect of different defect depths and defect diameters on the surface temperature difference of the specimen.

As shown in fig. 3(a), for defects with the same diameter, the temperature difference between the presence and absence of defects will gradually increase over time, and the shallower the defect depths, the more significant the temperature difference. According to fig. 3(b), it appears that when the depths of the defect are the same, the larger the defect diameters, the more obvious the temperature difference.

Image sequence processing

Processing algorithms

Inter frame differential-multi frame cumulative average method

Inter frame differential method is to obtain the outline of defects by performing a differential operation on two adjacent frames in an infrared thermal image sequence [7]. The original image sequence is $\{I_1(a, b),..., I_{x-1}, (a, b), I_x(a, b)\}$. The new image sequence obtained by sequentially performing first-order differencing on each frame according to eq. (3) is $\{P_1(a, b), P_2(a, b),..., P_{x-1}(a, b)\}$:

$$P_{x-1}(a,b) = I_x(a,b) - I_{x-1}(a,b) \tag{2}$$

where (a, b) pixel position co-ordinates and x – the number of frames corresponding to the current image.

The residual images containing target defects and random noise are obtained after the image sequence is processed by inter frame differencing [8]. It is calculated as shown in:

$$\overline{P_i(a,b)} = \frac{1}{k}\sum_{i=1}^{k} P_i(a,b), \quad k \le x-1 \tag{3}$$

where $P_i(a, b)$ is the i^{th} frame image in the new image sequence obtained by inter-frame difference processing and k – the number of images processed by the cumulative average.

Figure 4 shows the processed image. According to fig. 4, the size, position and contour of defects in the image can be clearly identified, and the contrast between areas with and without defects is obvious, with little noise interference.

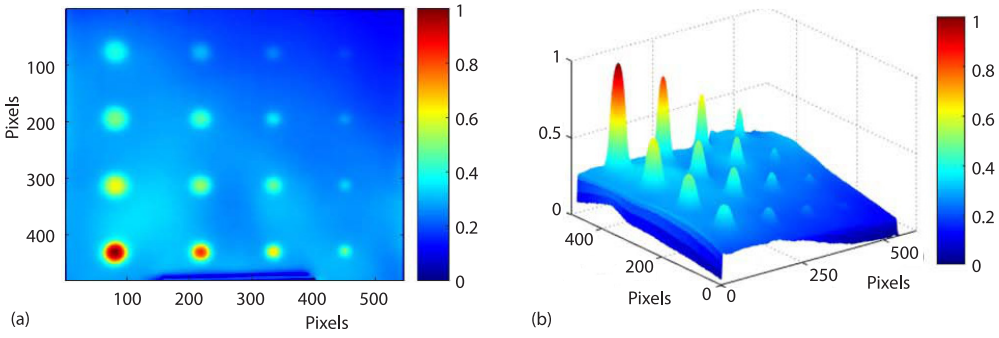

Figure 4. Results of FD-MCA; (a) 2-D graph and (b) 3-D graph

Polynomial fitting-correlation coefficient method

The polynomial fitting-correlation coefficient method (FCC) is to construct a set of the dataset based on the temperature value T_n corresponds to every pixel (x, y) in the image sequence at time, t_n. The polynomial model in the form of eq. (4) is used to perform curve fitting according to the least square method. The fitting image sequence can be obtained according to the fitting coefficient and time series [9]:

$$T(t) = \sum_{n=0}^{N} a_n t_n \tag{4}$$

where a_n is the fitting coefficient.

The original thermal image sequence was processed by FCC. It can be seen from fig. 5 that there are more defects shown in the second-order coefficient diagram and the outline of defects is clear. However, there are many noise points in the constant coefficient diagram.

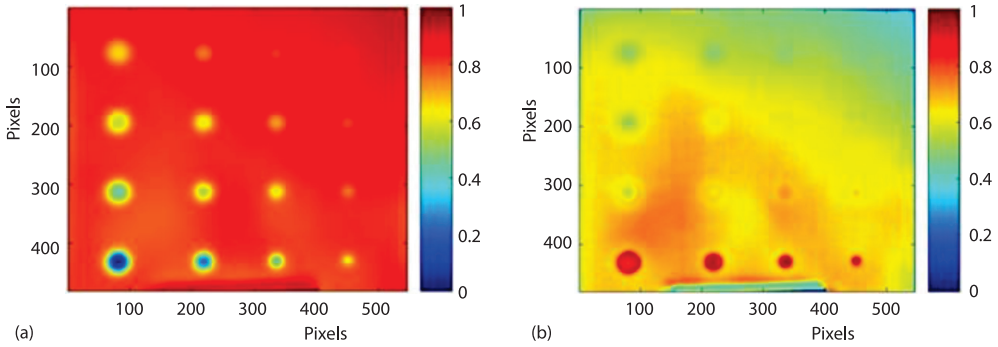

Figure 5. Results of FCC; (a) the coefficients of the second-order coefficient and (b) the coefficients of the constant coefficient

Time-difference contrast method

The time difference contrast method (TDC) can subtract the two frames produced at different times [10]. The two frames can be associated by a multiplicative scale factor α:

$$I_1 = \alpha I_2 \tag{5}$$

where I_1 and I_2 are the images at moments t_1 and t_2, respectively.

The two images are differentially processed:

$$I_d = \alpha I_2 - I_1 \tag{6}$$

where I_d is the differential image.

The image processed by the time difference comparison method is shown in fig. 6. According to the figure, we can find that although all defects can be identified, there is still a quantity of noise in the processed image.

Evaluation of algorithms

For comparing the effect of the aforementioned image sequence processing algorithms, this paper uses signal-to-noise ratio (SNR) and the information entropy (IE) to evaluate the best result of each algorithm.

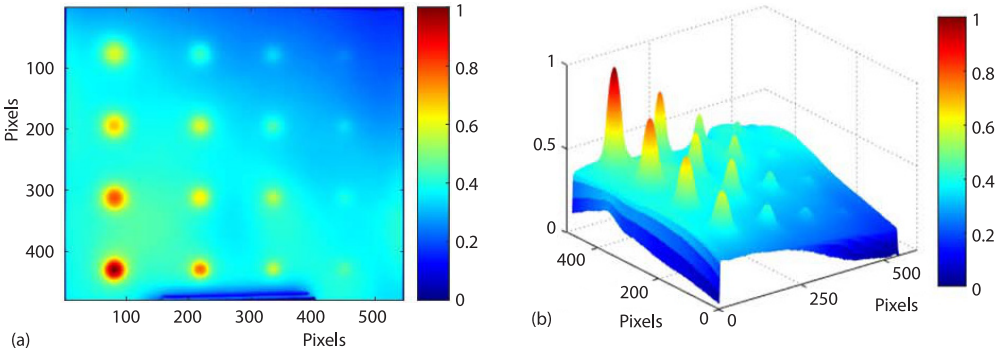

Figure 6. Results of TDC; (a) 2-D graph and (b) 3-D graph

The higher the SNR is, the less noise in the image is. The SNR reads as:

$$SNR = \frac{|E_d - E_{nd}|}{\sigma_{nd}} \tag{7}$$

where E_d is the mean pixel value of the defective areas, E_{nd} – the mean value of pixel value in the defect free areas, and σ_{nd} – the standard deviation of defect free areas.

The higher the information entropy, the richer the details of the defect features contained in the image [11]. The information entropy can be expressed:

$$IE = -\sum_{i=1}^{N}\left[E_i(x,y)\log_2 E_i(x,y)\right] \tag{8}$$

where $E_i(x, y)$ and $\log_2 E_i(x, y)$ are the frequency of occurrence of the corresponding gray value at a pixel point in the image in the whole image, and the logarithm of the frequency of occurrence of the corresponding gray value at a point.

The SNR and IE of the images processed by the aforementioned algorithms are computed and fig. 7(b) shows the outcomes. It can be found in the figure that the IE of the images processed by the three algorithms TDC, FCC, and FD-MCA are higher than that of the original thermal image. The SNR of the image processed by FCC and FD-MCA is significantly higher than that of the original image, indicating that the FCC and FD-MCA algorithms have a stronger ability to suppress noise.

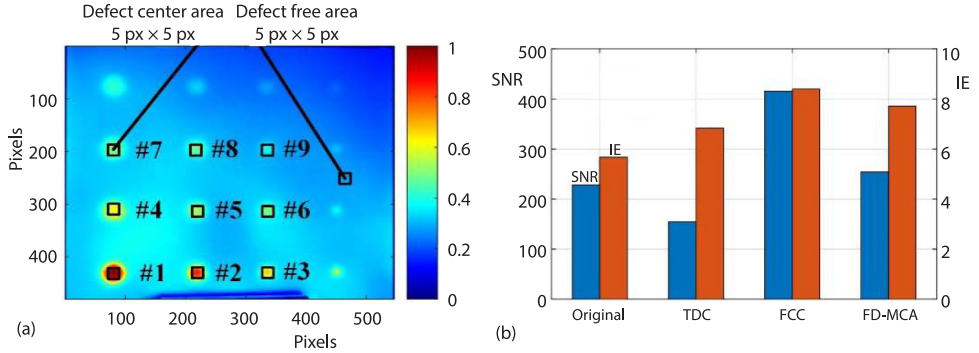

Figure 7. The SNR reference area and calculation of SNR and IE

Conclusion

For detecting debonding defects in GFRP laminates, a lock-in thermography inspection system was built, and the effect laws of diameters and depths of defects on surface temperature difference were discussed. The FD-MCA, FCC, and TDC were used to process the original image sequences, and the results show that FD-MCA, FCC, and TDC can improve the image quality, and the FCC algorithm has a stronger ability to suppress the noise, which can be more effective in the extraction of defect information.

Acknowledgment

This project is supported by Natural Science Foundation of Heilongjiang Province (Grant No. JQ2023E011).

Nomenclature

f – phase-locked frequency, [Hz]
q_0 – maximum heat flow, [Wm^{-2}]
$q(t)$ – heat flow from halogen lamps, [Wm^{-2}]
SNR – signal to noise ratio, [db]
t – scan period of the modulation signal, [second]
x, y – co-ordinates spaces, [m]

References

[1] Wu, P. H., Based on the Research and Development of Glass Fiber Composites for Wind Turbine Blades (in Chinese), *Synthetic Materials Aging and Application*, *50* (2021), 6, pp. 128-130
[2] Zhang, J., Non-Destructive Evaluation of Fiber-Reinforced Polymer Composites Using Terahertz Technology (in Chinese), Ph. D. thesis, Jilin University, Changchun, China, 2016
[3] Wei, J. C., *et al*., Research and Development Status of Infrared Thermal Imaging Non-Destructive Testing Technology, *Journal of Harbin University of Science and Technology*, *25* (2020), 2, pp. 64-72
[4] Zhang, W., *et al*., Infrared Thermal Wave Non-Destructive Technology on the Defect in the Shell of Solid Rocket Motor, *Proceedings of SPIE – The International Society for Optical Engineering*, *7* (2010), 6, pp. 30-34
[5] Liu, Y. T., *et al.*, The Development History, Current Status, and Trends of Infrared Thermal Imaging Non-Destructive Testing Technology (in Chinese), *Non-Destructive Testing*, *39* (2017), 8, pp. 63-70
[6] Liu, J. Y., *et al.*, The Study on Infrared Lock – In Thermography Technology Based on Image Sequences Processing, *Laser and Infrared*, (2008), 7, pp. 654-658
[7] Si, M. D., *et al.*, Infrared Small Target Detection Based on Saliency and Frame-to-Frame Difference, *Aerospace Electronic Warfare*, *31* (2015), 4, pp. 32-35
[8] Li, H. Q., *et al*., Application of Multi frame Accumulative Average Technology in Infrared Real Time Image Processing, *Laser and Infrared*, (2005), 12, pp. 978-982
[9] Zhang, X. B., Research on Fiber Metal Laminate Defects Detection Using Infrared Thermal Wave Non-Destructive Testing Technology (in Chinese), M. Sc. thesis, Harbin University of Commerce, Harbin, China, 2019
[10] Larsen, C., Document Flash Thermography, M. Sc. thesis, Utah State University, Logan, Ut., USA, 2011
[11] Jiang, D., *Information Theory and Coding*, University of Science and Technology of China Press, Hefei, China, 2004

Paper submitted: June 11, 2023
Paper revised: August 19, 2023
Paper accepted: November 10, 2023